Carnegie Observatories Astrophysics Series, Vol. 3:
Clusters of Galaxies: Probes of Cosmological Structure and Galaxy Evolution, 2004
ed. J. S. Mulchaey, A. Dressler, and A. Oemler (Cambridge: Cambridge Univ. Press)

The Red Sequence Technique and High-redshift Galaxy Clusters

MICHAEL D. GLADDERS
The Observatories of the Carnegie Institution of Washington

Abstract

The advent of large-format CCD cameras on 4 m-class telescopes has led to a resurgence of interest in using optical and near-IR images for detecting galaxy clusters over a range of redshifts. Parallel to the development of new observing strategies has been the development of a number of sophisticated algorithms to analyze these imaging data in order to optimally select real clusters. One of the most successful algorithms, particularly at high redshifts, has been the so-called red sequence method. This method keys on the observational fact that all clusters possess a population of passively evolving early-type galaxies that form an identifiable color sequence in a color-magnitude diagram. This paper reviews the recent history of the development and application of red sequence methods, with particular focus on results from the Red-Sequence Cluster Survey (RCS). This survey, currently the largest moderately deep imaging survey designed to use this method, is particularly useful since its volume and redshift depth are comparable to those of the largest distant cluster surveys done at other wavelengths.

1.1 Cluster Surveys

The utility of optical imaging data for surveying large areas for galaxy clusters was recognized early on, and is epitomized by the work of Abell (1958). Abell's initial ground-breaking cluster catalog spurred an enormous amount of research on galaxy clusters, motivating both a wide array of other surveys (see Bahcall 1977 for a more complete list of early optical cluster catalogs) and a great deal of detailed research on cluster properties. More recently, X-ray surveys have come to be recognized as the standard method for galaxy cluster surveys, particularly for more distant clusters (e.g., the Extended Medium Sensitivity Survey cluster sample, Gioia et al. 1990; the *ROSAT* Distant Cluster Survey, Rosati et al. 1998, to name but a few among many examples). X-ray surveys are particularly attractive since the observational signature of a galaxy cluster is unique at X-ray wavelength. This results quite directly in remarkably clean, uncontaminated cluster catalogs (the dominant source of contamination being blends of unresolved X-ray point sources; see Vikhlinin et al. 1998 for a discussion). The selection functions, and hence the effective survey volume, can be readily quantified in X-ray surveys and are robust (e.g., Adami et al. 2000). These two properties, low contamination and well-determined selection functions, are of critical importance in large surveys, since the statistical analyses envisioned for future clusters samples (e.g., Haiman, Mohr, & Holder 2001; Levine, Schulz, & White 2002) are expected to be dominated by systematic uncertainties. The known projection-induced contamination of early, optically selected cluster catalogs (e.g., Lucey 1983; van Haarlem, Frenk, & White 1997), and difficulties in a ready quantification of selection functions for such surveys, led to these surveys falling out of favor coincident with the advent of X-ray methods. However, the development of large-format CCD cameras and sophisticated analysis methods has begun to reverse this trend.

The first significant effort to use CCDs and a sophisticated cluster-finding algorithm in order to locate distant galaxy clusters was the Palomar Distant Cluster Survey (PDCS: Postman et al. 1996). The PDCS used the matched-filter algorithm, in which information on the radial position and luminosity distribution of galaxies is used to discriminate projections from real clusters. A number of authors have since revised or extended the initial algorithm of Postman et al., and current variants include the adaptive matched filter (Kepner et al. 1999) and the hybrid matched filter (Kim et al. 2002). The matched-filter method has been demonstrated to be most successful at lower redshifts, via application to Sloan Digital Sky Survey (SDSS) data. There has been little application at $z > 0.5$, and little confirmation of initial PDCS cluster candidates at these distant redshifts. This result is not unexpected; the change in $m - M^*$ with redshift is most pronounced at lower redshifts, and hence one generally expects the luminosity filter to be most effective at lower redshifts.

An alternate algorithm was suggested by Gladders & Yee (2000). This method, dubbed the cluster red sequence (CRS) algorithm, and described in detail below, implicitly uses the concentration of cluster galaxies at a particular color as a tracer. Variants of this basic method have since been outlined by other authors, mostly in the context of the SDSS. These color-based methods include the "cut-and-enhance" algorithm of Goto et al. (2002) and the "MaxBCG" method of Annis et al. (1999). All use color information in some way to discriminate real structures from projections. Comparisons of some of these algorithms as applied to the SDSS show that they perform comparably well and similarly to matched-filter methods (Kim et al. 2002) at low redshifts.

For more distant clusters, efficiency of data acquisition becomes paramount (since cluster galaxies get very faint), and so methods that rely on multiple-filter data (such as the "C4" algorithm; see Nichol 2004) are likely to be less attractive. In this regard, the matched-filter methods may be the most attractive, since in principle imaging in only a single filter is required. However, in practice, most matched-filter surveys have used imaging in at least two filters, with results cross-checked between different wavelengths (e.g., Postman et al. 1996; Olsen et al. 2001), with the only exception being the Deeprange Survey of Postman et al. (2002). Moreover, considerations for the secondary use of wide-field imaging data often make at least one more filter preferable.

Arguably the most efficient optical method, at least in identification of initial candidates, is the background light fluctuation method of Dalcanton (1996), as used in the Las Campanas Distant Cluster Survey (González et al. 2001). In this method clusters are initially identified as unresolved enhancements in the extragalactic background light, which can then be followed up using modest aperture telescopes to acquire deeper direct imaging to gather photometric information and estimate redshifts. However, the advent of large-field mosaic cameras, large enough that multiple clusters are seen in any one image, mitigates this advantage significantly. With large cameras it is more efficient to gather the deeper data directly in survey mode.

1.2 The CRS Method in Detail

The CRS algorithm detailed in Gladders & Yee (2000) relies on two–filter imaging data to select clusters. Clusters are isolated in a 4-dimensional space of position (x,y), magnitude (m), and color (c). Using models of the expected evolution of the cluster red sequence, the algorithm specifically targets early-type galaxies. These objects offer a number of potential advantages as cluster tracers. Early-type galaxies evolve passively with redshift, and are about one magnitude brighter at $z = 1$ compared to present epoch (e.g., Schade, Barrientos, & López-Cruz 1997; van Dokkum et al. 1998). The morphology-density relation (Dressler 1980; Dressler et al. 1997) shows that the early-type galaxies are the most clustered cluster members. The presence of a red sequence is also a physical indicator of overdensity, much like the thermal bremsstrahlung emission from clusters seen in X-rays. Additionally, in good-quality imaging data, these galaxies can be morphologically selected, further enhancing their clustering signal. Early-type galaxies also dominate the bright end of the luminosity function in most clusters (e.g., Barger et al. 1998). Finally, the photometric evolution of passively evolving stellar populations is readily modeled, and hence photometric redshifts and other secondary measurements based on these galaxies are likely to be accurate.

Most importantly, the use of the CRS algorithm and appropriate filters should completely eliminate foreground projection, and mitigate background projection as well. This is illustrated in Figure 1.1, which shows the $B-R$ versus R color-magnitude diagram (CMD) for the inner 0.5 h^{-1} Mpc of $\sim$40 low-redshift, X-ray selected Abell clusters, taken from the data of López-Cruz (1997). Each cluster CMD has been k-corrected to the mean redshift of the sample, but has not been background corrected. The red sequence is obvious. As shown in Figure 1.1, because these filters span the 4000 Å break at this redshift, all foreground galaxies whose intrinsic spectra are no redder than the cluster early-type galaxies appear bluer than the red sequence in this CMD. A simple blue-side color cut thus eliminates all foreground galaxies. Background galaxies may appear either bluer or redder, but are generally fainter. The intrinsically redder (presumably early-type) galaxies at higher redshift appear redder than the cluster red sequence. Thus, a simple red-side color cut eliminates the most clustered background galaxies. The remaining galaxies, in a narrow color slice, are predominantly early-type galaxies at a particular redshift, with some contamination at fainter magnitudes by intrinsically bluer galaxies at higher redshift. This simple isolation of galaxies at a particular redshift is readily achieved at any redshift, so long as the filter pair spans the 4000 Å break.

The suggested variants of both the matched-filter and red sequence-based methods described above are often motivated by a desire to reduce the level of parameterization and hence sensitivity to model choices. In this context, it is worth noting that a mismatch between the assumed red sequence model and the actual colors of cluster galaxies does little to detection sensitivity in the CRS algorithm. Rather, such mismatches are likely to affect, in a systematic way, the estimation of cluster parameters such as the redshift. Fundamentally, the fact that any given cluster has a tighter color distribution than the field, regardless of its redshift, is what makes the CRS and similar algorithms work. Moreover, a tight red sequence is not generally required in order to detect a given cluster; even red sequences with scatters of half a magnitude (much larger than seen in any actual clusters) are detectable, because the field color scatter is even larger, and hence a color cut still enhances such a cluster against the more diverse background.

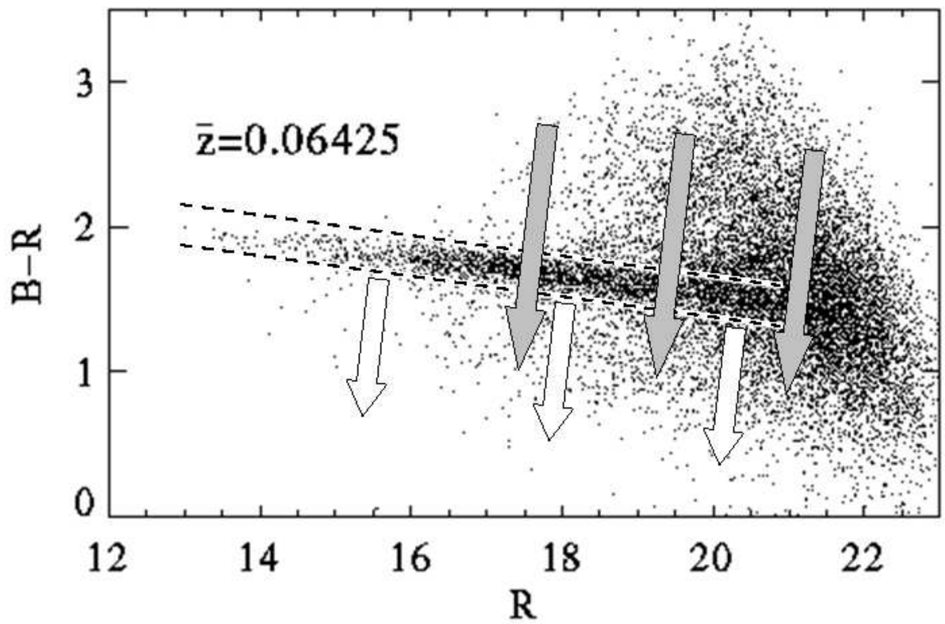

Fig. 1.1. Individual galaxies are shown as points. The red sequence of this aggregate cluster is obvious, and a narrow color slice bracketing it is shown by the dashed lines. The solid white arrows show the typical location of any normal galaxy foreground to the cluster, and the solid gray arrows similarly show the expected locations for background galaxies.

The CRS method has been tested in comparison to several other cluster-finding methods. A comparison to spectroscopically indicated structures in the CNOC2 survey (Yee et al. 2000) can be found in Gladders & Yee (2000), who showed that the method was able to delineate bound systems down to group sizes, had a contamination rate of 5% or less, even at these low mass thresholds, and provided quite precise redshift estimates. A preliminary study by Gladders & Donahue (2004) in several *ROSAT* Optical X-ray Survey (ROXS; Donahue et al. 2002) fields similarly shows that the CRS methods successfully finds all X-ray indicated structures. The most thorough analysis of the CRS method to date is by Gilbank (2003); his detailed comparison of the CRS method to both the matched-filter algorithm and X-ray selection shows that the CRS method is more complete and less contaminated by projection than the matched-filter method, and that it successfully recovers 100% of clusters that would be selected in an X-ray survey.

1.2.1 Redshift Estimates

Numerous authors, beginning with Visvanathan & Sandage (1977), have explored the possibility of using the details of the color-magnitude sequence as either a direct distance indicator, or more simply as a redshift indicator. This latter application is of interest in the context of cluster surveys since redshift and mass (the estimation of which usually depends

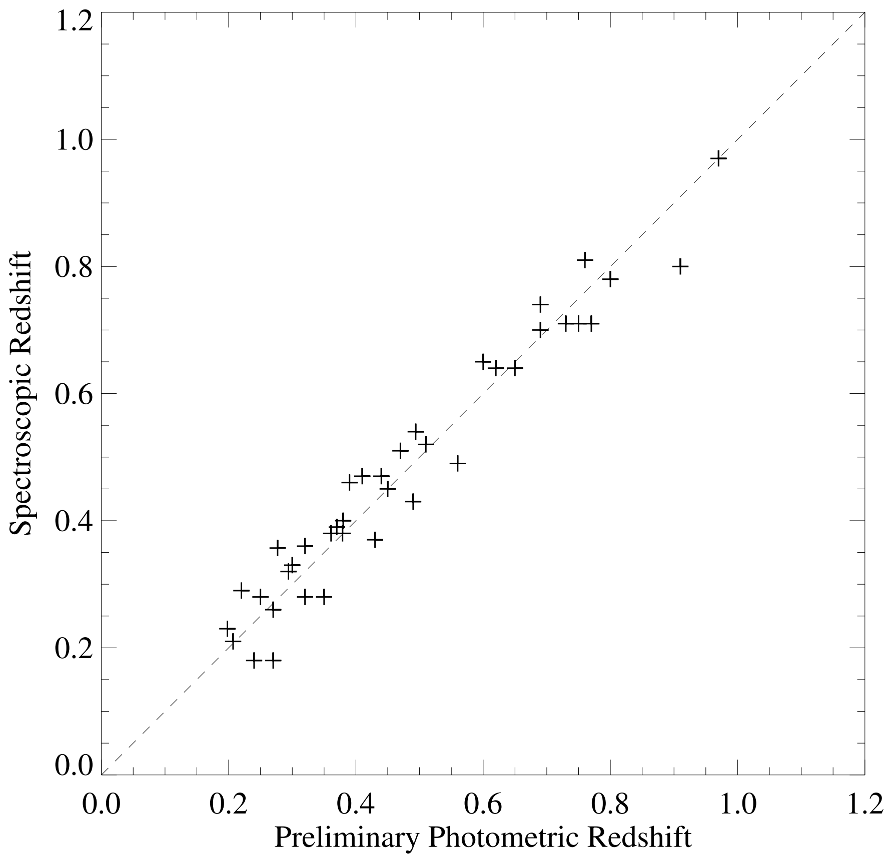

Fig. 1.2. A comparison of spectroscopic and photometric redshifts for an initial sample of 39 RCS cluster candidates. All clusters appear to be real (see the extensive discussion in Ellingson et al. 2004 for more details) and the photometric redshift uncertainty is about 0.05 across the entire sample. A restricted sample, consisting of clusters drawn only from patches with good photometric calibration, has a smaller redshift uncertainty of about 0.03.

on redshift) are the two most desirable basic properties to include in a cluster sample. The utility of the red sequence color as a redshift indicator has been noted at various redshifts. López-Cruz (1997), in a study of 45 Abell clusters mostly at $z < 0.1$, showed that the red sequence color provided a redshift estimate with an uncertainty of 0.008. Gladders & Yee (2000) similarly showed that the redshift uncertainty for poor systems at $0.12 < z < 0.55$ was 0.026. Smail et al. (1998), in a study of 10 X-ray selected clusters at $0.2 < z < 0.3$, similarly concluded that the red sequence provides an excellent and economical redshift indicator. Gilbank (2003) also examined the redshift estimates from both the matched-filter and CRS algorithms, and concluded that the CRS algorithm provides a much better redshift estimate.

As shown in Figure 1.2, recent spectroscopy of clusters in the RCS (Ellingson et al. 2004) also illustrates the accuracy of the CRS redshift estimates. For clusters up to $z = 0.97$ (the highest-redshift RCS clusters with spectroscopic confirmation; see Barrientos et al. 2004) the CRS method provides redshifts with uncertainties less than 0.05, and as good as 0.03 in fields with final photometric calibration (Ellingson et al. 2004). With filters spanning the 4000 Å break at moderate redshift, the color change in magnitudes is roughly equal to the change in redshift, and hence a systematic cluster-to-cluster calibration uncertainty of only a few hundredths of a magnitude per filter (likely better than many extragalactic imaging projects) completely explains this scatter.

It is also worth noting that at higher redshifts the fundamental redshift accuracy achievable by this simple color-based method may be limited by uncertainties in the process of early-type galaxy formation. Figure 1.3 shows the likely effect of mismatches between the model used to compute redshifts and the actual scenario for formation of the cluster red sequence. Two lines are plotted, showing the systematic redshift error induced by using a simple instantaneous burst model with the burst formed at $z_f = 2.5$, when used to infer redshifts for clusters with actual formation redshifts of $z_f = 2$ and $z_f = 3$. In both cases there are systematic offsets in redshift that are less than about 0.01 at redshifts less than 0.8, increasing to offsets as large as 0.2 at the highest redshifts considered. At $z > 1$, the potential systematic redshift errors are thus likely to be at least as large as the random errors, and may well dominate. This dramatic increase in the redshift uncertainty is due to the small time difference between the observation epoch and formation epoch, and the bluing of the survey filters in the rest frame. This latter effect can be eliminated by reimaging the highest-redshift cluster candidates using redder filters. Moreover, the correct model can be chosen by calibrating to clusters with known redshifts. However, if the formation redshifts of clusters are stochastically distributed, then calibration of the photometric models to known clusters will not eliminate this extra source of uncertainty.

1.3 The Red Sequence and Cluster Confirmation

The detection of a red sequence in a cluster candidate selected by other means is arguably the observationally cheapest way to confirm the cluster identification. The data necessary to show a red sequence are modest in scope, and for even very distant systems can be readily acquired. Indeed, it is in the most distant clusters, to date typically selected by faint X-ray emission, where many of the arguments for the universality of the red sequence arise (Gladders & Yee 2000). Examples of clusters selected by a variety of means that show significant red sequences include X-ray selected clusters at $z > 1$ in the *ROSAT* Distant Cluster Survey (Rosati et al. 1999; Stanford et al. 2002; Holden et al. 2004), and $z \approx 1$ clusters selected using the matched-filter method applied to the ESO Imaging Survey (e.g., da Costa et al. 1999). The presence of an overdensity of red galaxies has been used extensively to argue for the presence of clusters around a number of distant AGNs (e.g., Dickinson 1995; Hall & Green 1998; Tanaka et al. 2000; Haines et al. 2001; Blanton et al. 2004) or to suggest the existence of clusters of galaxies associated with absorption-line complexes seen in the spectra of a background AGN (Liu et al. 2000). Lubin et al. (2000) used the presence of a spatially extended red sequence population to identify large-scale structure, on the super-cluster scale, associated with the $z \approx 0.91$ clusters Cl 1604+4304 and Cl 1604+4321.

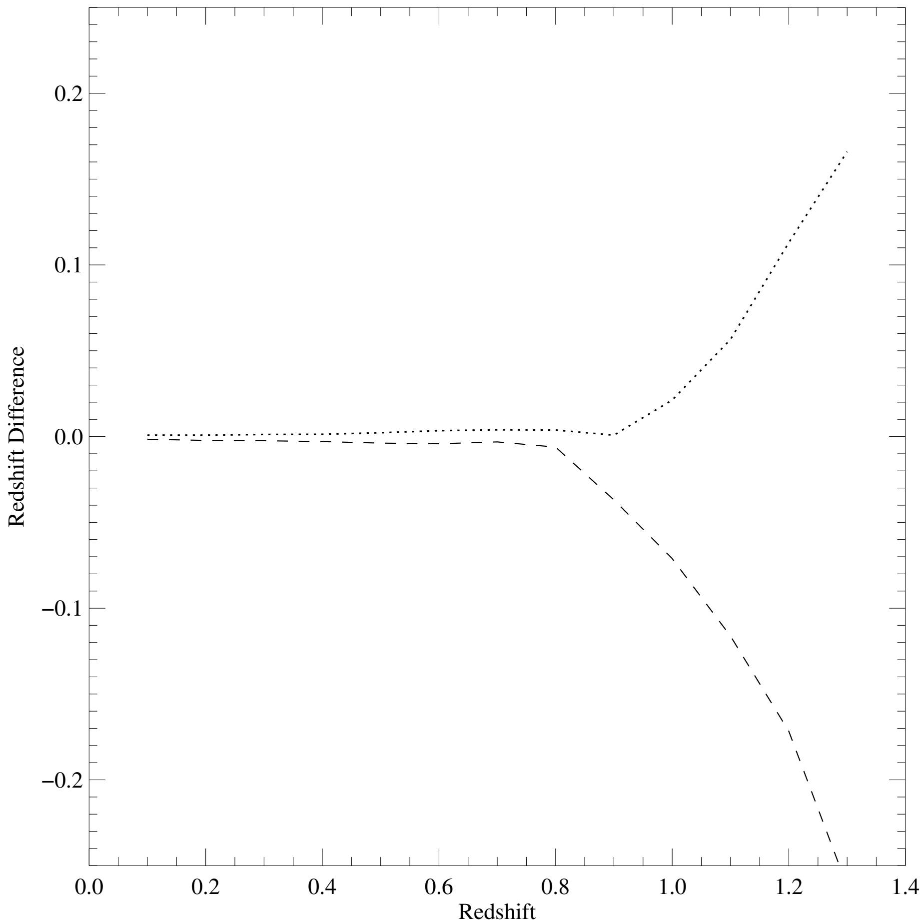

Fig. 1.3. The lines show the expected systematic redshift errors for mismatches between the actual red sequence models as compared to the fiducial model used in the CRS algorithm. The difference in estimated redshifts for $z_f = 2$ (dashed line) and $z_f = 3$ (dotted line) models when compared to the $z_f = 2.5$ model is illustrated.

1.4 The Red Sequence Cluster Survey

1.4.1 Survey Data and Design

The Red-Sequence Cluster Survey (RCS: Gladders 2002; Gladders & Yee 2004) is a $\sim$100 square degree R_C and z' imaging survey designed to detect and characterize galaxy clusters out to the redshift limits allowed by standard CCDs. In practice, the quickly falling response of CCDs at near-infrared wavelengths limits the bulk of the RCS cluster sample to below $z = 1.1$, with a tail of cluster candidates out to $z = 1.4$. The imaging for the RCS was carried out at the Canada-France-Hawaii Telescope (CFHT) from mid-1999 to early-2001, and at the Cerro Tololo Interamerican Observatory's (CTIO) 4 m telescope from early-2000 to late-2001. In both cases observations were made with large-format mosaic cameras—the

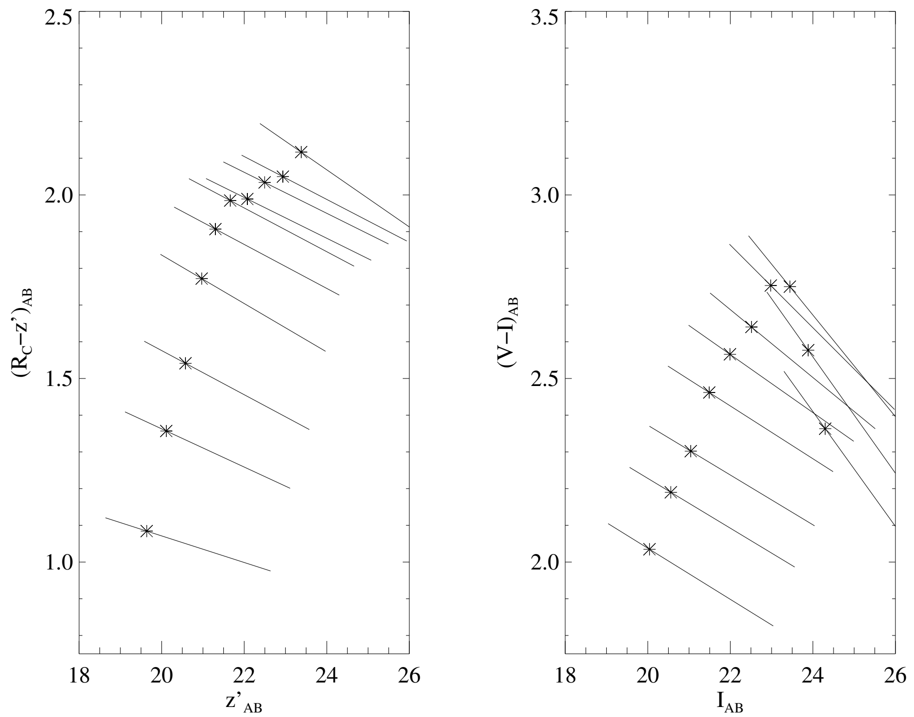

Fig. 1.4. Fiducial red sequences for cluster early-type galaxies at $0.5 < z < 1.4$, in steps of 0.1 in redshift, using the RCS R_C and z' filter pair (*left*) and the V and I filter pair (*right*) often used in previous optical cluster surveys. The star symbols indicate the location of M^* at each redshift.

CFH12K at CFHT (Cuillandre et al. 2000) and MOSAIC-II on the CTIO 4 m. Both data sets are of similar depth in both filters—with integration times anywhere from 12 to 25 minutes per filter—with 5 σ point source limits typically being two magnitudes past M^* at $z = 1$, for an early-type galaxy model with passive evolution. The CFHT data mostly have excellent seeing of 0.″6–0.″8; the CTIO data are of more typical ground-based image quality, but similar in depth due to the larger aperture of the telescope and increases in exposure time. The RCS required, in total, 25 clear nights to complete, making it a remarkably efficient cluster survey given its total volume.

The RCS data were designed to optimally and efficiently sample the galaxy cluster population at moderate to high redshifts. As shown in Figure 1.4, the redshifts of early-type galaxies in these clusters are much better sampled by the R_C and z' filters, compared to the typical choice of V and I filters often used in other surveys (e.g., Postman et al. 1996; Donahue et al. 2002). On the other hand, the RCS redshift estimates at lower redshifts (less than $z = 0.5$) are less accurate than can be achieved using a bluer filter pair. Compare, for example, the redshift uncertainty of $\sim$0.05 seen in Figure 1.2 with the uncertainty of $\sim$0.026 found in an application of the CRS algorithm to CNOC2 $V-I$ data by Gladders &

Table 1.1. *Parameters for Simulated Clusters in RCS Tests*

Parameter	Symbol	Model Values	Notes
cluster redshift	z	0–1.4	
Abell Richness counts	$N_{\rm Abell}$	35,44,56,72,93,120	Richness Classes 0–2
blue fraction	$f_{\rm b}$	0.1,**0.45**,0.65,0.8,0.9	
NFW core scale radius	$r_{\rm s}$	0.1,0.2,**0.3**,0.4,0.5	in h^{-1} Mpc
ellipticity	ϵ	0.0,0.2,**0.4**,0.6,0.8	ϵ at 1 h^{-1} Mpc
red seq. formation redshift	$z_{\rm RS}$	2.0,**2.5**,3.0	lower limit in redshift
scatter in age prior to $z_{\rm RS}$	$\Delta t_{\rm RS}$	0.5,**1.0**,max	top-hat width in Gyr
LF R-band M^*	M_R^*	–22.75, **–22.25**, –21.75	$\alpha = -1.0$, $H_0 = 50$

The range or set of values used is indicated, with the “typical” value (if there is one) in boldface type.

Yee (2000). Recall, however, that in either filter pair two-filter photometric redshifts derived from colors are significantly more accurate than other methods.

1.4.2 Selection Functions

It has been argued for years that one of the attractions of X-ray selected samples is the relative simplicity of the selection functions for X-ray clusters. Landmark efforts to thoroughly model X-ray cluster selection functions range from the resampling treatment of Rosati et al. (1995), to the extensive Monte Carlo treatment of Vikhlinin et al. (1998), with the extensive and now complex simulations of the SHARC Survey by Adami et al. (2000) being the latest standard in this work. By no means are the Adami et al. simulations simple, and recent data on various X-ray selected samples (e.g., Lewis et al. 2002; Jones et al. 2004) clearly show that the complexity of the Adami et al. simulations is required to fully understand the selection functions for distant X-ray cluster populations.

In tandem with this realization of the actual complexity of X-ray cluster selection has been a growth in simulation methods to address the long-acknowledged complexity of optical selection. Complications in optical selection are obvious; depending on the method, optical surveys may be sensitive to details of the luminosity function, the radial galaxy distribution, the cluster ellipticity, details of the galaxy population, and evolution of these properties across both redshift and mass. This is in addition to selection effects induced by the characteristics of the observations, which are generally more complex (factoring in different filters, seeing, image depths, variations in depths, etc.) than the observational effects in X-ray data (primarily flux limits and spatial point-spread function variations). Nevertheless, several large surveys have now completed extensive modeling of optical selection functions. One notable example is the modeling of SDSS clusters sample, discussed in Nichol (2003). The particular advantage offered by the SDSS is that the “mock” catalogs used to measure the selection effects are very well constrained by the extensive SDSS data, and hence offer a thorough and robust platform in which to explore the effects of variations in a host of cluster properties, as well as variations due to different cluster-finding algorithms. At these redshifts the optical selection functions are at least as well constrained as X-ray selection functions.

A similar effort to model the RCS selection functions, using only the CRS algorithm (Gladders 2002; Gladders & Yee 2004), is illustrated in Figure 1.5. This shows a synopsis

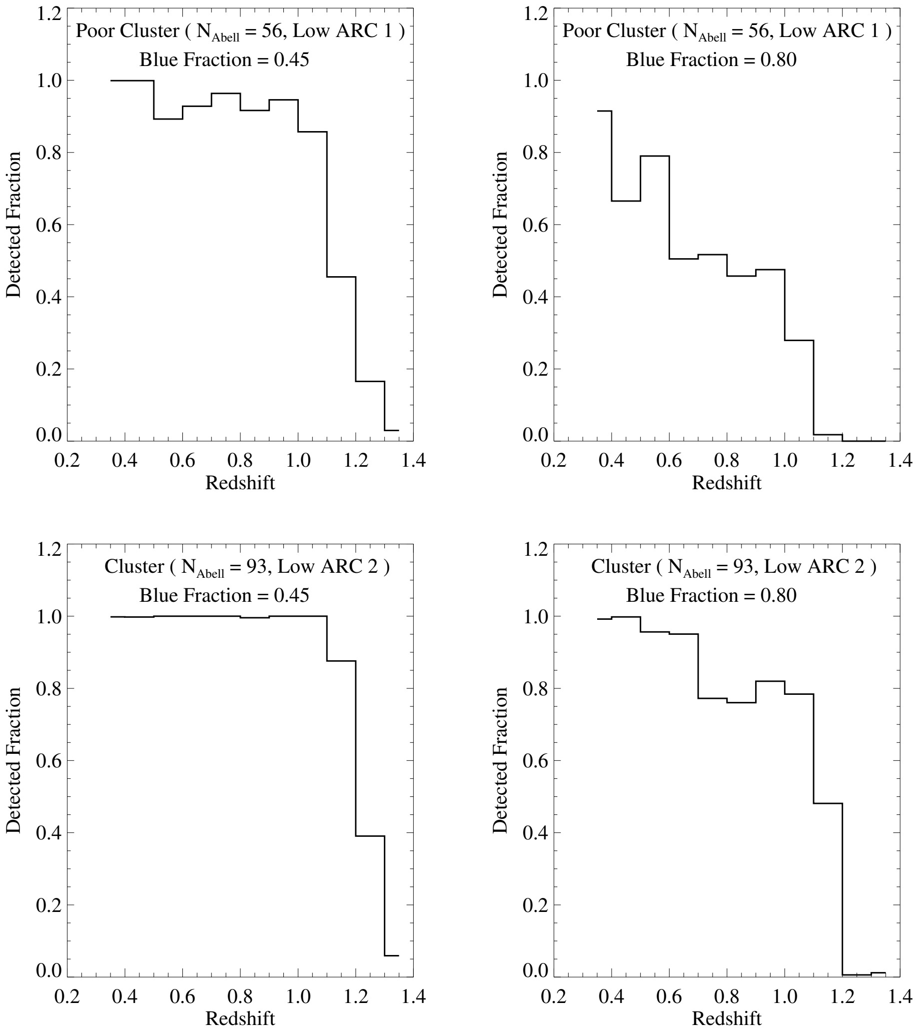

Fig. 1.5. The four panels show the recovered fraction of clusters in simulations for four representative clusters types, as indicated on each panel. Parameters not mentioned assume the standard value indicated in Table 6.1. Uncertainties due to the limited number of simulations are of order 5%–10%, as suggested by the variance in the plots.

of the predicted detection rates of a few sets of typical clusters: both moderately poor and rich clusters, with both moderate and high blue fractions, over the redshift range 0.3 – 1.4. These simulations explored variations in a number of parameters possibly relevant for cluster detection; a listing of the parameters, as well as the range explored in each, can be found in Table 6.1. The variation in these parameters was chosen to more than bracket all existing observations of clusters, and hence generally include extremal models (very rich systems at low redshift with high blue fractions, for example), which do not appear to exist in the

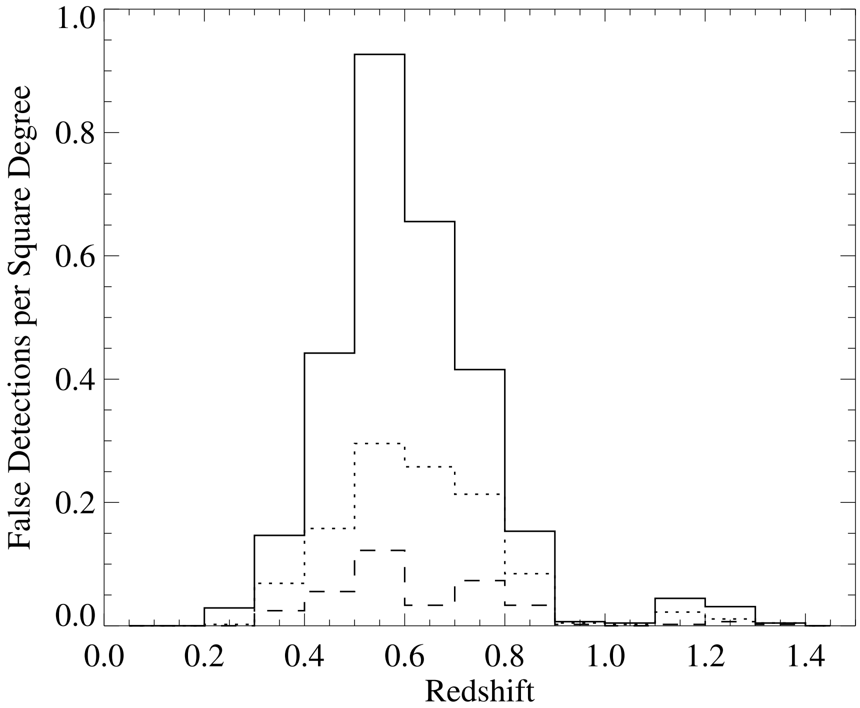

Fig. 1.6. The redshift histograms show the number of false-positive detections, per square degree, for selection thresholds of 3.0, 4.0, and 4.5 σ.

Universe. Clusters were embedded in realistic, evolving field galaxy models deduced from a combination of the CNOC2 survey's intermediate-redshift luminosity function (Lin et al. 1999) and a host of other magnitude, redshift, and color distributions from other surveys (see Gladders 2002 and Gladders & Yee 2004 for details). The field galaxies were spatially arranged to produce the observed CNOC2 correlation functions (Shepherd et al. 2001) using the simple algorithm of Soneira & Peebles (1978), but do not reflect in detail the higher-order clustering of clusters seen in the real Universe.

A simple synopsis of these extensive tests is that the RCS is expected to be 100 percent complete for galaxy clusters of richnesses equivalent to Abell Richness Class (ARC) 1 or greater (or, equivalently, of velocity dispersions $\geq$ 700 km s^{-1}; Yee & Ellingson 2003) to redshifts up to $z \approx 1.1$, with blue fractions as high as 0.65, regardless of the details of the spatial arrangement of the cluster. Yet higher blue fractions, generally higher than almost all observations, introduce some incompleteness above $z \approx 0.7$, for clusters with richnesses up to ARC 2; for the most massive clusters, with velocity dispersions in excess of 1000 km s^{-1}, the RCS should be complete to at least $z = 1.1$ regardless of all details of the galaxy population, provided that the optical mass-to-light ratios are within reason.

The false-positive rates for the RCS derived from these simulations are shown in Figure 1.6. Results are shown for three different significance cuts; for comparison, the signif-

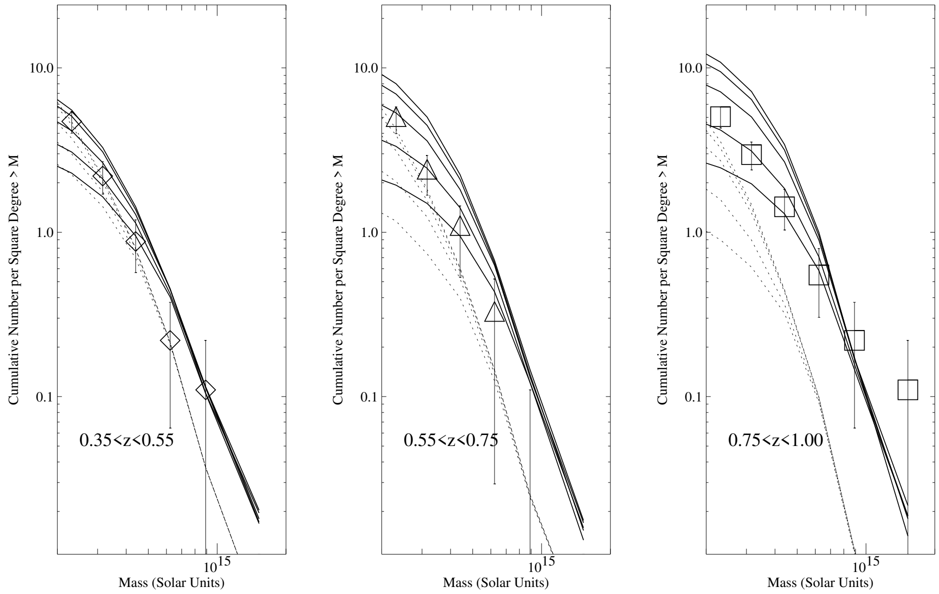

Fig. 1.7. The three panels show the deduced RCS cumulative cluster mass function in three redshift intervals, as indicated, from 2×10^{15} to 2×10^{14} $M_{\odot}$. The lower mass limit corresponds to the low end of Abell Richness Class 0. Solid lines show the predicted mass functions for the ΛCDM Virgo simulations, for various cluster blue fractions (0.1, 0.45, 0.65, 0.8 and 0.9). In general the data match the ΛCDM expectation quite well, particularly considering that the blue fraction is expected to evolve to higher values at higher redshifts. The dotted lines show the predicted mass functions for the τCDM Virgo simulations. τCDM is a much poorer fit to the data.

icance cut used previously in the selection functions in Figure 1.5 is 3 σ. Based on initial analyses of the RCS data, the false-positive rate at the 3 σ cut translates to about 5% contamination in real data. Note that this does not include contamination due to nearby projected structures, i.e. multiple groups along the same line of sight, with redshift separations less than the redshift uncertainty (see Fig. 1.2). However, even at twice the quoted contamination, the RCS has contamination rates competitive with X-ray surveys (e.g., Vikhlinin et al. 1998).

1.4.3 The RCS Mass Function

A preliminary measurement of the RCS mass function, using two of 20 survey patches and a galaxy richness-mass calibration derived from the CNOC1 survey (Yee & Ellingson 2003), is shown in Figure 1.7. RCS data are shown with random errors only, and are compared to an estimate of the mass distribution derived from the Virgo Hubble Volume simulations* (Evrard et al. 2002).

To make the comparison, we have taken the catalog of simulated cluster redshifts and

* The simulations used in this paper were carried out by the Virgo Supercomputing Consortium using computers based at the Computing Centre of the Max-Planck Society in Garching and at the Edinburgh Parallel Computing Centre. The data are publicly available at `http://www.mpa-garching.mpg.de/NumCos`.

velocity dispersions from the Virgo simulations and applied the RCS selection functions to predict which of the simulated clusters would be detected in a survey similar to the RCS. The richness-σ_1 relation deduced from the CNOC1 catalog (richness parameterized here by $B_{\rm gc}$; see Yee & Ellingson 2003) is used to produce a $B_{\rm gc}$ value for each simulated cluster that is detected. The observed run of $B_{\rm gc}$ errors with redshift and $B_{\rm gc}$ in the real data is then used to randomly perturb the simulation $B_{\rm gc}$ values. Finally, we convert both the real and simulated $B_{\rm gc}$ measurements to virial masses, again using the relation from CNOC1. This last change is essentially cosmetic and serves simply to translate richness to more familiar masses.

The RCS data agree well with the predictions for a flat ΛCDM cosmology with $\Omega_{\rm m} = 0.3$ and disagree with expectations for a $\Omega_{\rm m} = 1.0$ τCDM cosmology. This is not unexpected given the wealth of other indicators favoring the former model (e.g., Spergel et al. 2003, and references therein). Note that in this comparison the range of redshifts considered ($0.35 < z < 1.0$) is well beyond the redshift range of the mass-calibrating sample ($0.15 < z < 0.55$), and so conclusions about cosmology based on the higher redshift evolution of the mass function must be made with care. Work is ongoing to extend the CNOC1 calibration to $z = 1$ using RCS clusters.

1.4.4 RCS High-redshift Clusters

Little is currently known about galaxy clusters at redshifts beyond 1. Detailed descriptions of several of the most notable clusters at $z \geq 1$ can be found in, for example, Holden et al. (2004) and Rosati (2004), but the current sample size of fewer than a dozen known clusters at these redshifts limits the global conclusions that can be drawn from these investigations. One of the primary goals of the RCS is to enable a more thorough study of high-redshift clusters by providing samples of hundreds, rather than handfuls, of target systems. An ongoing project using the Las Campanas telescopes is following up the 100 best RCS high-redshift cluster candidates. The basic data are deep I-band imaging with the Magellan telescopes, coupled to K-band imaging of matching depth from the du Pont Telescope. The observations are designed to be both deeper and redder than the initial RCS survey data.

An initial analysis of the first 12 candidates imaged in both filters yields the following basic results.

(1) The RCS false-positive rate at $z \geq 1$ is 10%–20%. This is somewhat higher than the nominal contamination rates discussed above, but not unexpected given recent observations of strong clustering in extremely red galaxies with colors corresponding to early-type galaxies at high redshift (Daddi et al. 2002). This strong evolution of the red galaxy correlation function was not included in the background models, and would produce more false-positive detections.

(2) The red sequence galaxies in the apparently real clusters display much greater photometric variation than is observed in the few massive clusters studied at similar redshifts (Stanford, Eisenhardt, & Dickinson 1998; van Dokkum et al. 2000) and display scatter more comparable to that seen in cluster candidates associated with AGNs (e.g., Tanaka et al. 2000). The richest and hence most massive clusters have photometric properties similar to that seen in clusters in the literature (see Barrientos et al. 2004) and similarly small color scatter, but poorer systems often show much larger scatter. A pair of CMDs for two clusters at $z \approx 1$ is shown in Figure 1.8; one cluster is massive (see the discussion on strong lensing below) and has a low scatter of ≤ 0.1 magnitudes in $I - K$, while the other cluster, of about half the

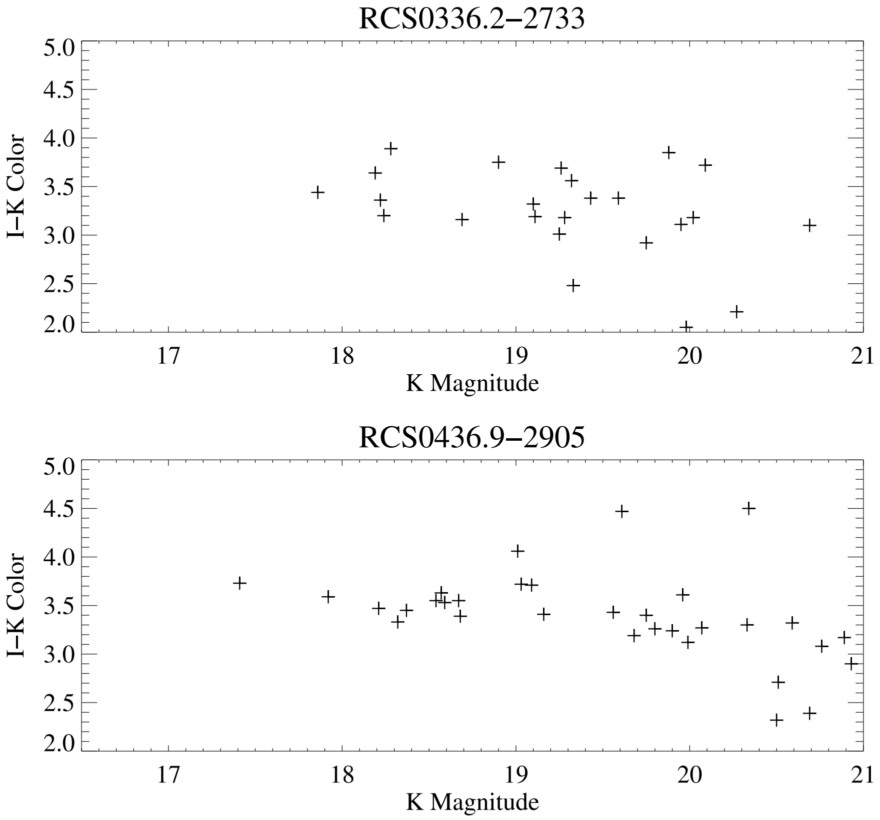

Fig. 1.8. The $I-K$ CMDs of two RCS clusters at $z \approx 1$ are shown. The cluster at the top is poorer and has a red sequence with a larger color scatter than the richer cluster at the bottom.

richness, has a scatter of ~ 0.25 magnitudes. Under the standard interpretation (e.g., Bower, Lucey, & Ellis 1992), in which the color scatter is related to a combination of star formation synchronicity between galaxies and the age of galaxies, this indicates that the galaxies in the less massive clusters are either younger or have a more diverse star formation history. This has not been seen in prior studies, likely because the available targets at $z \geq 1$ from previous clusters surveys were limited to the few most massive clusters in a given survey volume. Notably, these results are broadly consistent with expectations from hierarchical clustering models, in which the seeds of galaxies in the densest portions of the Universe are thought to collapse first.

(3) The reddest red sequences seen to date are approximately one magnitude redder in $I-K$ than the spectroscopically confirmed $z = 0.97$ cluster RCS0439.6–2905 (Barrientos et al. 2004), and hence the RCS sample includes cluster candidates with photometric redshifts as distant as $z = 1.4$. Only a handful of such ultra-distant systems are expected in the 100 clusters follow-up, based on the selection functions discussed above.

Finally, note that initial analysis of *Chandra* data (discussed in detail in Hicks et al. 2004) on a variety of RCS clusters with redshifts estimated or spectroscopically confirmed to be in the range $0.65 < z < 1.3$ indicates some X-ray emission in all cases. Though these clusters are often underluminous in X-rays with respect to more local X-ray-optical correlations derived from X-ray selected cluster samples, the presence of X-rays in all cases verifies the efficacy of the CRS method, even at high redshift.

1.4.5 RCS Strong Lensing Clusters

One of the most striking initial results of the RCS is the large number of high-redshift lensing clusters seen in the survey (Gladders et al. 2003; Gladders, Yee, & Ellingson 2002). A total of five clusters with one or more arcs are seen in RCS survey data, with an additional three strong lensing clusters selected from the 100 cluster follow-up of $z \geq 1$ cluster candidates discussed above. Images of lensing clusters from both the primary and secondary samples are shown in Figures 1.9 and 1.10. Apart from the clear verification that the RCS does detect massive clusters, this sample of strong lensing clusters is particularly notable for two reasons. First, the redshift distribution of the primary sample is skewed toward higher redshifts, with all five clusters at $0.64 < z < 0.87$. Standard considerations for lensing by clusters leads to the expectation that most strong lens clusters should be at lower redshifts, since clusters at lower redshift are thought to be more massive and are geometrically favored for lensing. Thus, the absence of RCS lensing clusters at $z < 0.64$ indicates that something in addition to mass, likely associated with cluster formation, is boosting the lensing cross sections of these systems. Secondly, in both the primary and secondary sample there is a high proportion of multiple-arc clusters, again implying that the systems that do have lensing have large lensing probabilities. The physical cause of this lensing boost is at present unclear.

The redshift distribution seen in the RCS lenses is also interpretable as a very clear detection of evolution in the cluster population, albeit in a property other than simply mass. Evolution has been notoriously hard to detect in X-ray surveys (e.g., Holden et al. 2004, and references therein). This points to one of the potential advantages and complications of optical cluster surveys—that they tend to find a broad range of systems, not just those with strong X-ray emission. Or, put another way, optical cluster surveys probe much deeper into the mass function than X-ray surveys. When trying to understand questions of cluster evolution, this is a desirable feature.

One final implication of this result is that clusters with arcs likely represent a sample that is structurally biased. That is, the density profiles of such systems are likely not typical, and this makes it questionable whether detailed studies of individual lens systems (e.g., Treu 2004) can be used to probe clusters in general.

1.5 Summary and Future Directions

The future of optical surveys for galaxy clusters looks bright. At low redshifts the SDSS is providing an wealth of detailed information that will serve to anchor surveys toward higher redshifts. Multiple methods for filtering optical data to search for real clusters have been tested at lower redshifts, and many appear to work well. At higher redshifts the most successful method to date appears to be the CRS method, which keys on the excess of red galaxies seen in all clusters studied so far.

Photometric redshift estimates for clusters using only two filters are demonstrated to work well over the redshift range $0 < z < 1$. Testing of this in detail at higher redshifts awaits a larger sample of clusters with spectroscopy. At high redshifts, systematic effects due to vari-

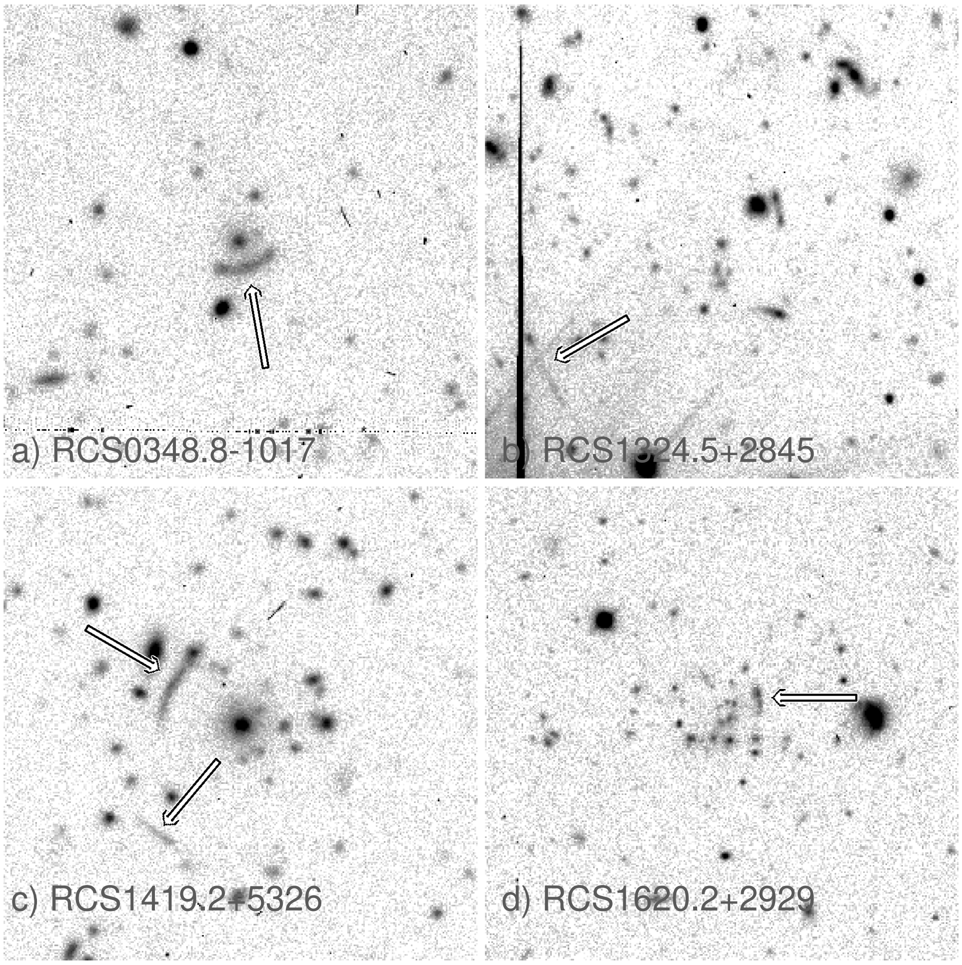

Fig. 1.9. The four panels show greyscale R_C-band images of the central $1' \times 1'$ of the four lensing clusters in the primary sample. A fifth cluster is described in detail in Gladders et al. (2002). The putative arc features are indicated by an arrow in each case.

ations in formation histories may be the limiting factor for this simple redshift estimator, and at low redshifts the achievable accuracy is limited by systematic uncertainties in photometric calibration.

Calculations of selection functions for optically selected clusters are now as developed as those for X-ray selection. At higher redshifts, a lack of detailed data on many clusters sets some limits on the robustness of these calculations (a point that can be argued for X-ray selection as well), though new investigations will surmount this limitation shortly. Lingering concerns about the robustness of red sequence-based methods for finding high-blue fraction clusters have not yet been thoroughly addressed, though the computed selection functions include these effects and indicate that large blue fractions are only significant (in the RCS at

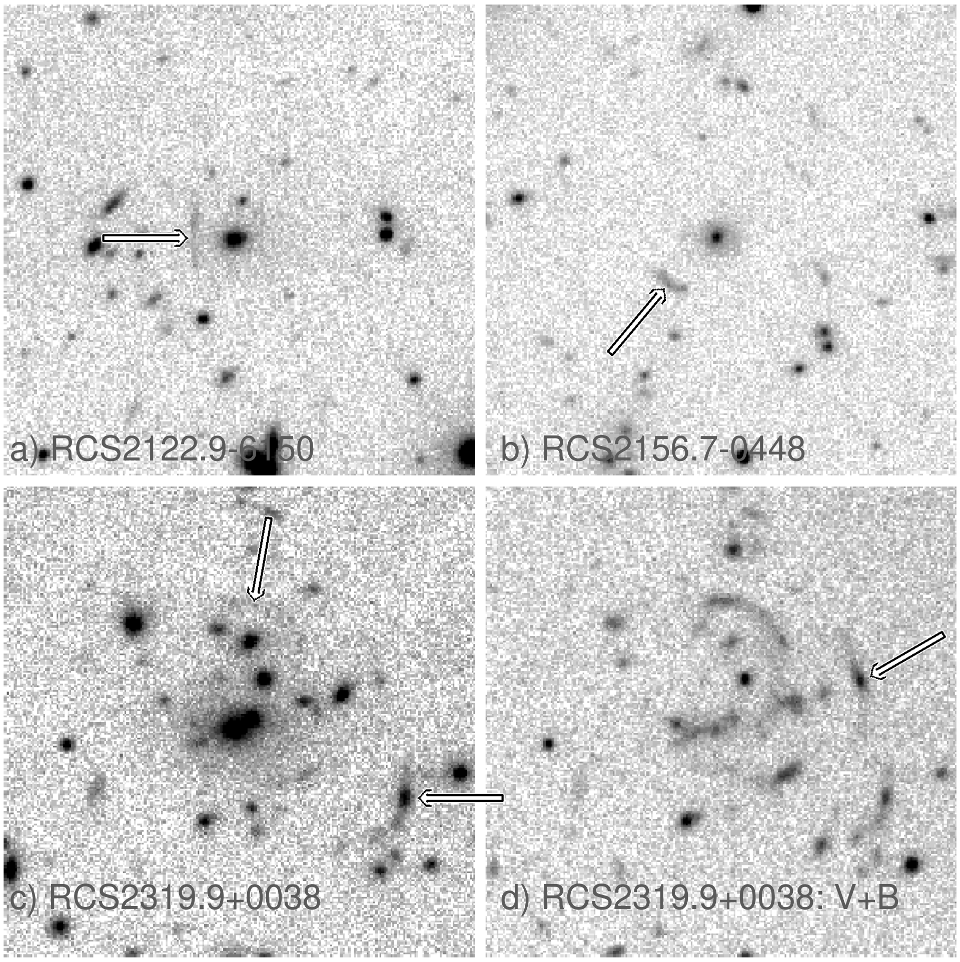

Fig. 1.10. Panels (*a*)–(*c*) show greyscale *I*-band images of the central $30'' \times 30''$ of the three lensing clusters in the secondary sample. The putative arc features are indicated by an arrow in each case. Panel (*d*) shows RCS2319.9+0038 in *V* and *B* light, from a summed image in which the arcs have similar signal-to-noise ratio in each filter.

least) for less massive systems with blue fractions in excess of 0.65—larger than indicated by most data.

The low contamination and high completeness of red sequence-based methods suggested by simulations is well borne out by observations. Cross comparison of X-ray selection and red sequence selection demonstrates that no X-ray selected clusters would be missed by this form of optical selection. Follow-up of the RCS, even to the highest redshifts in the RCS catalogs ($z \approx 1.4$) shows contamination rates comparable to X-ray selection.

Clusters have for some time been one of the prime targets for cosmological investigations, because the growth of clusters is thought to be extremely sensitive to parameters such as Ω_m and σ_8. Current discussions in the literature suggest that extremely large-area, high-redshift cluster surveys are needed in order to answer the most pressing cosmological questions. The demonstrated ability of red sequence-based cluster surveys to effectively find and characterize a clean cluster sample to very high redshifts makes such surveys an excellent tool for addressing these cosmological questions. To this end, a second-generation red sequence survey, envisioned as a 1000 square degree survey with selection functions similar to the RCS, is now underway at the CFHT. Coincident surveys at other wavelengths are highly desirable, and we plan to make the field locations for this next survey available soon in order to encourage other investigators to overlap with this survey. Unresolved questions regarding the efficacy of different methods for cluster selection, and, more importantly, questions regarding the correlations between mass-related observables, are best addressed using large, overlapping survey areas across a broad range of wavelengths.

Acknowledgements. It is a great pleasure to thank my RCS collaborators for their valuable insights and support during the RCS project. In particular, I am grateful to Howard Yee, Felipe Barrientos, Erica Ellingson, and Pat Hall for their strong involvement in this large project, without which it simply would not have happened. I am also grateful to my collaborators for allowing me to discuss several new RCS results in this review, prior to their publication elsewhere.

References

Abell, G. O. 1958, ApJS, 3, 211
Adami, C., Ulmer, M. P., Romer, A. K., Nichol, R. C., Holden, B. P., & Pildis, R. A. 2000, ApJS, 131, 391
Annis, J., et al. 1999, BAAS, 195, 1202
Bahcall, N. A. 1977, ARA&A, 15, 505
Barger, A. J., et al. 1998, ApJ, 501, 522
Barrientos, L. F., Manterola, M. C., Gladders, M. D., Yee, H. K. C., Infante, L., Hall, P., & Ellingson, E. 2004, in Carnegie Observatories Astrophysics Series, Vol. 3: Clusters of Galaxies: Probes of Cosmological Structure and Galaxy Evolution, ed. J. S. Mulchaey, A. Dressler, & A. Oemler (Pasadena: Carnegie Observatories, http://www.ociw.edu/ociw/symposia/series/symposium3/proceedings.html)
Blanton, E., Gregg, M. D., Helfand, D. J., Becker, R. H., & White, R. L. 2004, in Carnegie Observatories Astrophysics Series, Vol. 3: Clusters of Galaxies: Probes of Cosmological Structure and Galaxy Evolution, ed. J. S. Mulchaey, A. Dressler, & A. Oemler (Pasadena: Carnegie Observatories, http://www.ociw.edu/ociw/symposia/series/symposium3/proceedings.html)
Bower, R. G., Lucey, J. R., & Ellis, R. S. 1992, MNRAS, 254, 589
Cuillandre, J.-C., Luppino, G. A., Starr, B. M., & Isani, S. 2000, SPIE, 4008, 1010
da Costa, L. N., et al. 1999, A&A, 343, L29
Daddi, E., et al. 2002, A&A, 384, L1
Dalcanton, J. J. 1996, ApJ, 466, 92
Dickinson M. 1995, in A Fresh View of Elliptical Galaxies, ed. A. Buzzoni, A. Renzini, & A. Serrano (San Francisco: ASP), 283
Donahue, M., et al. 2002, ApJ, 569, 689
Dressler, A. 1980, ApJ, 236, 351
Dressler, A., et al. 1997, ApJ, 490, 577
Ellingson, E., et al. 2004, in preparation
Evrard, A. E., et al. 2002, ApJ, 573, 7
Gilbank, D. 2003, Ph.D. Thesis, Univ. Durham
Gioia, I. M., Henry, P. J., Maccacaro, T., Morris, S. L., Stocke, J. T., & Wolter, A. 1990, ApJ, 356, L35
Gladders, M. D. 2002, Ph.D. Thesis, Univ. of Toronto
Gladders, M. D., & Donahue, M. 2004, in preparation
Gladders, M. D., Hoekstra, H., Yee, H. K. C., Hall, P. B., & Barrientos, L. F. 2003, ApJ, 593, 48
Gladders, M. D., & Yee, H. K. C. 2000, AJ, 120, 2148
——. 2004, in preparation

Gladders, M. D., Yee, H. K. C., & Ellingson, E. 2002, AJ, 123, 1
González, A. H., Zaritsky, D., Dalcanton, J. J., & Nelson, A. 2001, ApJS, 137, 117
Goto, T., et al. 2002, AJ, 123, 1807
Haiman, Z., Mohr, J. J., & Holder, G. P. 2001, ApJ, 553, 545
Haines, C. P., Clowes, R. G., Campusano, L. E., & Adamson, A. J. 2001, MNRAS, 323, 688
Hall, P. B., & Green, R. F. 1998, ApJ, 507, 558
Hicks, A., et al. 2004, in preparation
Holden, B. P., Stanford, A., Rosati, P., Eisenhardt, P., & Tozzi, P. 2004, in Carnegie Observatories Astrophysics Series, Vol. 3: Clusters of Galaxies: Probes of Cosmological Structure and Galaxy Evolution, ed. J. S. Mulchaey, A. Dressler, & A. Oemler (Pasadena: Carnegie Observatories, http://www.ociw.edu/ociw/symposia/series/symposium3/proceedings.html)
Jones, L. R., Maughan, B. J., Ebeling, H., Scharf, C., Perlman, E., Limb, D., Gondoin, P., Mason, K. D., Cordova, F., & Priedhorsky, W. C. 2004, in Carnegie Observatories Astrophysics Series, Vol. 3: Clusters of Galaxies: Probes of Cosmological Structure and Galaxy Evolution, ed. J. S. Mulchaey, A. Dressler, & A. Oemler (Pasadena: Carnegie Observatories, http://www.ociw.edu/ociw/symposia/series/symposium3/proceedings.html)
Kepner, J., Fan, X., Bahcall, N., Gunn, J., Lupton, R., & Xu, G. 1999, ApJ, 517, 78
Kim, R. S. J., et al. 2002, AJ, 123, 20
Levine, E. S., Schulz, A. E., & White, M. 2002, ApJ, 577, 569
Lewis, A. D., Stocke, J. T., Ellingson, E., & Gaidos, E. J. 2002, ApJ, 566, 744
Lin, H., Yee, H. K. C., Carlberg, R. G., Morris, S. L., Sawicki, M., Patton, D. R., Wirth, G., & Shepherd, C. W. 1999, ApJ, 518, 533
Liu, M. C., Dey, A., Graham, J. R., Bundy, K. A., Steidel, C. C., Adelberger, K., & Dickinson, M. 2000, AJ, 119, 2556
López-Cruz, O. 1997, Ph.D. Thesis, Univ. of Toronto
Lubin, L. M., Brunner, R., Metzger, M. R., Postman, M., & Oke, J. B. 2000, ApJ, 531, L5
Lucey, J. R. 1983, MNRAS, 204, 33
Nichol, R. C. 2004, in Carnegie Observatories Astrophysics Series, Vol. 3: Clusters of Galaxies: Probes of Cosmological Structure and Galaxy Evolution, ed. J. S. Mulchaey, A. Dressler, & A. Oemler (Cambridge: Cambridge Univ. Press), in press
Olsen, L. F., et al. . 2001, A&A, 380, 460
Postman, M., Lauer, T. R., Oegerle, W., & Donahue, M. 2002, ApJ, 579, 93
Postman, M., Lubin, L. M., Gunn, J. E., Oke, J. B., Hoessel, J. G., Schneider, D. P., & Christensen, J. A. 1996, AJ, 111, 615
Rosati, P. 2004, in Carnegie Observatories Astrophysics Series, Vol. 3: Clusters of Galaxies: Probes of Cosmological Structure and Galaxy Evolution, ed. J. S. Mulchaey, A. Dressler, & A. Oemler (Cambridge: Cambridge Univ. Press), in press
Rosati, P., Della Ceca, R., Burg, R., Norman, C., & Giacconi, R. 1995, ApJ, 445, L11
Rosati, P., Della Ceca, R., Norman, C., & Giacconi, R. 1998, ApJ, 492, L21
Rosati, P., Stanford, S. A., Eisenhardt, P. R., Elston, R., Spinrad, H., Stern, D., & Dey, A. 1999, AJ, 118, 76
Schade, D., Barrientos, L. F., & López-Cruz, O. 1997, ApJ, 477, L17
Shepherd, C. W., Carlberg, R. G., Yee, H. K. C., Morris, S. L., Lin, H., Sawicki, M., Hall, P. B., & Patton, D. R. 2001, ApJ, 560, 72
Smail, I., Edge, A. C., Ellis, R. S., & Blandford, R. D. 1998, MNRAS, 293, 124
Soneira, R. M., & Peebles, P. J. E. 1978, AJ, 83, 845
Spergel, D. N., et al. 2003, ApJS, 148, 175
Stanford, S. A., Eisenhardt, P. R., & Dickinson, M. 1998, ApJ, 492, 461
Stanford, S. A., Holden, B., Rosati, P., Eisenhardt, P. R., Stern, D., Squires, G., & Spinrad, H. 2002, AJ, 123, 619
Tanaka, I., Yamada, T., Aragón-Salamanca, A., Kodama, T., Miyaji, T., Ohta, K., & Arimoto, N. 2000, ApJ, 528, 123
Treu, T. 2004, in Carnegie Observatories Astrophysics Series, Vol. 3: Clusters of Galaxies: Probes of Cosmological Structure and Galaxy Evolution, ed. J. S. Mulchaey, A. Dressler, & A. Oemler (Cambridge: Cambridge Univ. Press), in press
van Dokkum, P. G., Franx, M., Kelson, D., Illingworth, G. D., Fisher, D., & Fabricant, D. 1998, ApJ, 504, L17
van Dokkum, P. G., Franx, M., Fabricant, D., Illingworth, G. D., & Kelson, D. 2000, ApJ, 541, 95
van Haarlem, M. P., Frenk, C. S., & White, S. D. M. 1997, MNRAS, 287, 817
Vikhlinin, A., McNamara, B. R., Forman, W., Jones, C., Quintana, H., & Hornstrup, A. 1998, ApJ, 502, 558
Visvanathan, N., & Sandage, A. 1977, ApJ, 216, 214

Yee, H. K. C., et al. 2000, ApJS, 129, 475
Yee, H. K. C., & Ellingson, E. 2003, ApJ, 585, 215